INTERNATIONAL JOURNAL FOR NUMERICAL METHODS IN FLUIDS
Int. J. Numer. Meth. Fluids 2002; **40**:799–819 (DOI: 10.1002/fld.372)

A fast Godunov method for the water-hammer problem

Yao-Hsin Hwang[1] and Nien-Mien Chung[2,*,†]

[1] *Chung Shun Institute of Science and Technology, Lung Tan 90008-15-1, Tao-Yuan 32526, Taiwan*
[2] *Power Research Institute, Taiwan Power Company, 84, Da-An Rd., Shu-Lin, Taipei County, Taiwan*

SUMMARY

An efficient Godunov-type numerical method with second-order accuracy was developed to simulate the water-hammer problem in piping. The exact solutions of the Riemann problem were analysed and illustrated on the intriguing solution diagram by properly introducing dimensionless variables within reasonably practical ranges. Based on the solution diagram, an efficient fast Riemann solver was also developed. Moreover, small perturbation analysis was performed to demonstrate the relations between the primitive variables, velocity and pressure, for the Riemann problem. The typical shock-tube problem and the water-hammer problem were implemented as sample ones to test the numerical method. It was shown that the present numerical method incorporated with Van Leer's flux limiter is a promising one to simulate fluid transient problem for piping in the present study. Copyright © 2002 John Wiley & Sons, Ltd.

1. INTRODUCTION

Water-hammer is an important aspect in the designs or operations of piping system in power plants. The diagnoses of the problem are usually done by the aid of numerical method due to the complexity of the piping system. Method of characteristic (MOC) is one of the most popular numerical methods that are utilized in the analyses of the water-hammer problem because of its simplicity. The fundamentals of MOC and many practical applications can be referenced in the book [1]. Strictly speaking, however, MOC is not suitable to predict wave propagation correctly, especially for the wave with finite strength. One of the incentives of the paper is to develop an efficient numerical method which could avoid some shortcomings of MOC, such as the limitation of Courant number being unity, the linearization of the governing equations and accuracy, etc., at the expense of CPU time. The total efficiency however, can be amended by the fantastic progressing computer hardware for practical engineering purposes.

Besides MOC, many numerical methods had been proposed to simulate a variety of water-hammer problems [2, 3]. However, to capture accurate wave structures and characteristics,

*Correspondence to: N.-M. Chung, Power Research Institute, Taiwan Power Company, 84, Da-An Rd., Shu-Lin, Taipei County, Taiwan.
†E-mail: u076075@taipower.com.tw

Contract/grant sponsor: Taiwan Power Company

Received January 2001
Revised January 2002

Copyright © 2002 John Wiley & Sons, Ltd.

shock-capturing method by which the Rankine–Hugoniot relation is satisfied is one of the alternatives. Among them, the Godunov method is one of the most famous and important candidates. However, to implement the Godunov method to simulate wave propagation, the solution for the local Riemann problem at the cell interfaces has to be determined [4]. The solution of the Riemann problem in the gas dynamics is well understood and can be referred to the work by Sod [5]. Iterations are always necessary to solve the Riemann problem and then causes lower numerical efficiency. Besides developing an efficient numerical method, the other incentive of the present paper is to shed light on the fast Riemann solver for the water-hammer problem because of the simplicity of the governing equations. Under the properly selected dimensionless parameters, an intriguing solution diagram of the Riemann problem is proposed to demonstrate all the possible solutions for reasonably practical ranges. A fast Riemann solver is then constructed from the solution diagram and incorporated into the Godunov method to improve computational efficiency. The approximate Riemann solvers such as the Roe's and Osher's schemes are another approach to avoid iterations in solving the Riemann problem. To validate the present fast Riemann solver, the famous Roe's scheme is also utilized to serve this purpose [6].

The contents of this article are arranged as follows: governing equations and characteristic analysis are briefly discussed in Section 2, the Godunov method and the Riemann problem in Section 3. The fast Riemann solver based on the solution diagram is discussed in Section 4. To get a clear understanding between the pressure and velocity in the Riemann problem, a small perturbation analysis is also included. The numerical method and error analysis are discussed in Sections 5 and 6, the test problems and computational results in Section 7, and finally conclusions are delivered in Section 8.

2. GOVERNING EQUATIONS AND CHARACTERISTIC ANALYSIS

Considering the mass and momentum equation for one-dimensional horizontal pipe flow without friction:

$$\frac{\partial \rho}{\partial t} + \frac{\partial (\rho u)}{\partial x} = 0 \tag{1a}$$

$$\frac{\partial (\rho u)}{\partial t} + \frac{\partial (\rho u^2 + p)}{\partial x} = 0 \tag{1b}$$

where ρ is density, u the velocity and p is the pressure, while t and x denotes time and space, respectively. Equation (1) can be written in the compact form

$$\frac{\partial U}{\partial t} + \frac{\partial F}{\partial x} = 0 \tag{2}$$

The vector U contains two conservative variables $(\rho, \rho u)$ and the flux vector $F(\rho u, \rho u^2 + p)$. Equation (2) is equivalently represented as

$$\frac{\partial U}{\partial t} + A \frac{\partial U}{\partial x} = 0 \tag{3}$$

Copyright © 2002 John Wiley & Sons, Ltd.

where $A \equiv \partial F/\partial U$, is the Jacobian matrix and in the form

$$A = \begin{pmatrix} 0 & 1 \\ c^2 - u^2 & 2u \end{pmatrix}$$

where $c \equiv \sqrt{\mathrm{d}p/\mathrm{d}\rho}$ is the sound velocity.

The eigenvalue and eigenvector are easily obtained by diagonalizing the Jacobian matrix and Equation (3) is then casted into two mutually independent equations as

$$\frac{\partial W}{\partial t} + \Lambda \frac{\partial W}{\partial x} = 0 \tag{4a}$$

and

$$\delta W = R^{-1} \delta U \tag{4b}$$

where R is the matrix of eigenvector, Λ the diagonal matrix of eigenvalue and W is the characteristic variable. The eigenvalues corresponding to the characteristic variable are wave speed. As a result, two properties are summarized under the assumption of constant sound speed:

(1) along the line

$$\frac{\mathrm{d}x}{\mathrm{d}t} = u - c, \quad c \ln \rho - u = \text{constant} \tag{5a}$$

(2) along the line

$$\frac{\mathrm{d}x}{\mathrm{d}t} = u + c, \quad c \ln \rho + u = \text{constant} \tag{5b}$$

And, $(c \ln \rho - u,\ c \ln \rho + u)$ are just the components of the characteristic variable W. However, the characteristic relations are only appropriate for the smoothing flow field and are no more valid for the flow with sharp gradient, shock for instance [6]. Consequently, integral form of the mass and momentum equations, i.e. the Rankine–Hugoniot relation, shall be applied:

$$\sigma(\rho_{\mathrm{L}} - \rho_{\mathrm{R}}) = \rho_{\mathrm{L}} u_{\mathrm{L}} - \rho_{\mathrm{R}} u_{\mathrm{R}} \tag{6a}$$

$$\sigma(\rho_{\mathrm{L}} u_{\mathrm{L}} - \rho_{\mathrm{R}} u_{\mathrm{R}}) = \rho_{\mathrm{L}} u_{\mathrm{L}}^2 - \rho_{\mathrm{R}} u_{\mathrm{R}}^2 + p_{\mathrm{L}} - p_{\mathrm{R}} \tag{6b}$$

where σ is the shock speed, and subscripts L and R indicate the state before and after the shock wave.

3. THE GODUNOV METHOD AND RIEMANN PROBLEM

The Godunov method can be derived from the conservation form of Equation (2)

$$U_i^{n+1} = U_i^n - \frac{\Delta t}{\Delta x}(F_{i+1/2} - F_{i-1/2}) \tag{7}$$

Copyright © 2002 John Wiley & Sons, Ltd.

where $U_i^n \equiv 1/\Delta x \int_{x_{i-1/2}}^{x_{i+1/2}} U(x, n\Delta t)\,\mathrm{d}x$ is defined as the space-averaged state variable over the computational cell $(i-\frac{1}{2}, i+\frac{1}{2})$ and $F_{i+1/2} = 1/\Delta t \int_{n\Delta t}^{(n+1)\Delta t} F(x_{i+1/2}, t)\,\mathrm{d}t$ the time-averaged flux at the interface $i+\frac{1}{2}$. The key element of the numerical scheme is to determine the flux at cell interface $F_{i+1/2}$. The Godunov's method divides the domain of flow field into many computational cells with interfaces at which state variables are discontinuous. Then, the evolution from the initial discontinuity at interface has to be solved in each time step to determine the numerical flux in Equation (7) since

$$F_{i+1/2}^G = F(U_{i+1/2}^G)$$

where G denotes the Godunov method and $U_{i+1/2}^G$ is the exact solution of Equation (2) with discontinuous initial conditions. Thus, the Riemann problem for the present case is a model problem of Equation (2) with initial conditions

$$U(x,0) = \begin{cases} U_\mathrm{L}, & x < 0 \\ U_\mathrm{R}, & x > 0 \end{cases}$$

From the characteristic analysis, there are two characteristic lines for the system equations. It is known that shock results from the intersections of the same set of characteristic lines from different positions, while expansion fan from the characteristic lines which depart from each other. Generally speaking, the solutions of the Riemann problem can be split into three regions of constant states, which are determined by the wave patterns constituted through the interactions between two sets of characteristic lines. The complete solutions of the Riemann problem, including intermediate states, shock speed and the states within expansion wave, can be derived from the characteristic equation and the Rankine–Hugoniot relation [4, 7].

The interactions between the characteristic lines may result in shock or expansion fan and then there are four types of wave patterns for the Riemann problem as shown in Figure 1: (I) expansion fan–intermediate state–shock wave, (II) shock wave–intermediate state–shock wave, (III) shock wave–intermediate state–expansion fan and (IV) expansion fan–intermediate state–expansion fan. The boundaries of the wave patterns are determined by the appearance of shock wave or expansion fan. For example, the first type (I) and second type (II) of wave patterns are divided by the disappearance of expansion fan or shock wave on the left-hand side. That is $U_* = U_\mathrm{L}$ and the boundary of the first type (I) of wave pattern will be

$$\frac{u_\mathrm{L} - u_\mathrm{R}}{c} \leqslant \sqrt{\frac{\rho_\mathrm{L}}{\rho_\mathrm{R}}} - \sqrt{\frac{\rho_\mathrm{R}}{\rho_\mathrm{L}}}$$

For the same reason, the first type and the fourth type (IV) are separated by $U_* = U_\mathrm{R}$ and the boundary is

$$\frac{u_\mathrm{R} - u_\mathrm{L}}{c} \leqslant \ln \frac{\rho_\mathrm{L}}{\rho_\mathrm{R}}$$

Consequently, the ranges of the first type of wave pattern are completely defined. The ranges of other wave patterns can also be determined by the same approaches mentioned above. For convenience, the following dimensionless parameters are defined to determine the boundaries

Copyright © 2002 John Wiley & Sons, Ltd.

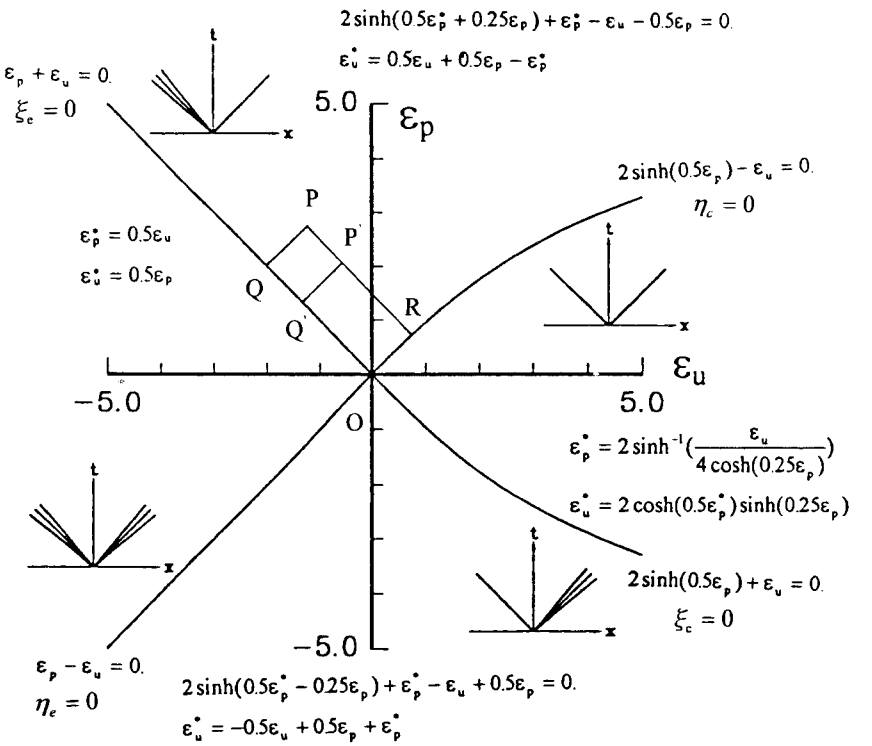

Figure 1. Four types of wave pattern of the Riemann problem and illustrations for the fast Riemann solver.

between wave patterns and the intermediate states:

$$\varepsilon_p = \ln \frac{p_{\mathrm{L}}}{p_{\mathrm{R}}}; \quad \varepsilon_u = \frac{u_{\mathrm{L}} - u_{\mathrm{R}}}{c}$$

$$\varepsilon_p^* = \ln \frac{p_*}{\sqrt{p_{\mathrm{L}} p_{\mathrm{R}}}}; \quad \varepsilon_u^* = \frac{u_* - (1/2)(u_{\mathrm{L}} + u_{\mathrm{R}})}{c}$$

The intermediate states of the four wave patterns are:

(1) Type I (expansion fan–intermediate state–shock)

$$\begin{aligned} 2\sinh(\tfrac{1}{2}\varepsilon_p^* + \tfrac{1}{4}\varepsilon_p) + \varepsilon_p^* - \varepsilon_u - \tfrac{1}{2}\varepsilon_p = 0 \\ \varepsilon_u^* = \tfrac{1}{2}\varepsilon_u + \tfrac{1}{2}\varepsilon_p - \varepsilon_p^* \end{aligned} \tag{11a}$$

(2) Type II (shock–intermediate state–shock)

$$\begin{aligned} \varepsilon_p^* &= 2\sinh^{-1}\left(\frac{\varepsilon_u}{4\cosh((1/4)\varepsilon_p)}\right) \\ \varepsilon_u^* &= 2\cosh(\tfrac{1}{2}\varepsilon_p^*)\sinh(\tfrac{1}{4}\varepsilon_p) \end{aligned} \tag{11b}$$

Copyright © 2002 John Wiley & Sons, Ltd.

(3) Type III (shock–intermediate state–expansion fan)

$$\begin{aligned} 2\sinh(\tfrac{1}{2}\varepsilon_p^* - \tfrac{1}{4}\varepsilon_p) + \varepsilon_p^* - \varepsilon_u + \tfrac{1}{2}\varepsilon_p = 0 \\ \varepsilon_u^* = -\tfrac{1}{2}\varepsilon_u + \tfrac{1}{2}\varepsilon_p - \varepsilon_p^* \end{aligned} \tag{11c}$$

(4) Type IV (expansion fan–intermediate state–expansion fan)

$$\begin{aligned} \varepsilon_p^* &= \tfrac{1}{2}\varepsilon_u \\ \varepsilon_u^* &= \tfrac{1}{2}\varepsilon_p \end{aligned} \tag{11d}$$

And, the boundaries of wave patterns are:

(1) types I and II

$$2\sinh(\tfrac{1}{2}\varepsilon_p) - \varepsilon_u = 0 \tag{12a}$$

(2) types II and III

$$2\sinh(\tfrac{1}{2}\varepsilon_p) + \varepsilon_u = 0 \tag{12b}$$

(3) types III and IV

$$\varepsilon_p - \varepsilon_u = 0 \tag{12c}$$

(4) types IV and I

$$\varepsilon_p + \varepsilon_u = 0 \tag{12d}$$

To directly illustrate the boundaries and intermediate states of wave patterns, all the possible solutions of the Riemann problem are rearranged in a solution diagram and demonstrated in Figure 1 within reasonable ranges of pressure and velocity. Besides the solutions of the intermediate states, other related solutions such as the propagation speeds of the waves are:

(1) for characteristic line, $\mathrm{d}x/\mathrm{d}t = u - c$

$$\begin{aligned} &\text{shock speed: } \tilde{\sigma}_\mathrm{l} = \tfrac{1}{2}\varepsilon_u - \mathrm{e}^{(1/2)\varepsilon_p^* - (1/4)\varepsilon_p} \\ &\text{speed of the rightmost characteristic line within expansion fan: } \tilde{s}_\mathrm{lr} = \varepsilon_u^* - 1 \\ &\text{speed of the leftmost characteristic line within expansion fan: } \tilde{s}_\mathrm{ll} = \tfrac{1}{2}\varepsilon_u - 1 \end{aligned} \tag{13a}$$

(2) for characteristic line, $\mathrm{d}x/\mathrm{d}t = u + c$

$$\begin{aligned} &\text{shock speed: } \tilde{\sigma}_\mathrm{r} = -\tfrac{1}{2}\varepsilon_u + \mathrm{e}^{(1/2)\varepsilon_p^* + (1/4)\varepsilon_p} \\ &\text{speed of the rightmost characteristic line within expansion fan: } \tilde{s}_\mathrm{rr} = 1 + \tfrac{1}{2}\varepsilon_u \\ &\text{speed of the leftmost characteristic line within expansion fan: } \tilde{s}_\mathrm{rl} = 1 + \varepsilon_u^* \end{aligned} \tag{13b}$$

Copyright © 2002 John Wiley & Sons, Ltd.

where superscript $\sim$ denotes dimensionless value and is defined as

$$\tilde{\sigma} = \frac{\sigma - (1/2)(u_{\mathrm{L}} + u_{\mathrm{R}})}{c}$$

In the Riemann problem, the shock wave or expansion fan generating from a single discontinuous interface will not intersect with each other. But they might interact with other waves from interfaces of neighbour cells in the real numerical problems. To avoid the interactions, the computational time step Δt has to be confined within the range

$$\frac{|\lambda|_{\max} \Delta t}{\Delta x} \leqslant 1$$

where subscript, max, stands for the maximum eigenvalue of all the interfaces of computation cells. This is the so-called Courant–Friedrichs–Lewy (CFL) condition and it is well known that the numerical scheme will be unstable if CFL condition is violated.

4. THE FAST RIEMANN SOLVER

It is obvious that the intermediate states shown in the solution diagram have to be solved by iterations for Types I and III. Since the solutions of the Riemann problem are necessary for each interface at all computational cells for the Godunov method, the computational efficiency is significantly reduced. To raise the efficiency, several approaches are proposed and discussed.

The first one is recasting the solution diagram of the Riemann problem over practical ranges into table form. Although the method is very straightforward, it has to utilize additional computational resources and the efficiency improved is limited.

The second approach is improving the initial guesses based on the solution diagram. As shown in Figure 1, iterations are essential only for the first and third wave patterns, while the intermediate states can be directly calculated for Types II and IV. It is also noted that the region of Type II is located within the range, $\varepsilon_u > 0$, and the region of Type IV within the range, $\varepsilon_u < 0$. As a result, the initial guesses of the iterations for Types I and III can be chosen as

$$\text{(i)}\ \varepsilon_u \geqslant 0, \quad \varepsilon_p^* = 2 \sinh^{-1}\left(\frac{\varepsilon_u}{4 \cosh((1/4)\varepsilon_p)}\right)$$

$$\text{(ii)}\ \varepsilon_u < 0, \quad \varepsilon_p^* = \tfrac{1}{2}\,\varepsilon_u$$

Namely, the intermediate state of Type II is implemented as the initial guess if $\varepsilon_u \geqslant 0$, while that of Type IV is selected if $\varepsilon_u < 0$. The converged solution can be obtained quickly by the Newton–Raphson method. The convergence criteria of ε_p^* in Equation (11) is

$$|2 \sinh(\tfrac{1}{2}\,\varepsilon_p^* + \tfrac{1}{4}\,\varepsilon_p) + \varepsilon_p^* - \varepsilon_u - \tfrac{1}{2}\,\varepsilon_p| \leqslant 10^{-7}$$

$$\left|\frac{\Delta \varepsilon_p^*}{\varepsilon_p^*}\right| \leqslant 10^{-4}$$

Copyright © 2002 John Wiley & Sons, Ltd.

where $\Delta\varepsilon_p^*$ is the difference between two successive iterations. Generally speaking, the iteration number to converge is no more than three if $\varepsilon_p \leqslant 3$ or $p_L/p_R \leqslant 20$.

The third approach, which is the most efficient one, is proposed hereafter. To illustrate the interesting properties of the solution diagram some dimensionless parameters are introduced and redefined:

$$\varepsilon_p(p_1, p_2) = \ln\frac{p_1}{p_2}; \quad \varepsilon_u(u_1, u_2) = \frac{u_1 - u_2}{c}$$

$$\varepsilon_{p,\mathrm{LR}} = \varepsilon_p(p_L, p_R); \quad \varepsilon_{p,*R} = \varepsilon_p(p_*, p_R); \quad \varepsilon_{p,L*} = \varepsilon_p(p_L, p_*)$$

$$\varepsilon_{u,\mathrm{LR}} = \varepsilon_u(u_L, u_R); \quad \varepsilon_{u,*R} = \varepsilon_u(u_*, u_R); \quad \varepsilon_{u,L*} = \varepsilon_u(u_L, u_*)$$

It is to be noted that there exists a relationship

$$\varepsilon_{p,\mathrm{LR}} = \varepsilon_{p,\mathrm{L}*} + \varepsilon_{p,*\mathrm{R}}; \quad \varepsilon_{u,\mathrm{LR}} = \varepsilon_{u,\mathrm{L}*} + \varepsilon_{u,*\mathrm{R}}$$

which can also be represented in a vector form,

$$\vec{\varepsilon}_{\mathrm{LR}} = \vec{\varepsilon}_{\mathrm{L}*} + \vec{\varepsilon}_{*\mathrm{R}} \tag{14}$$

where $\vec{\varepsilon}_{\mathrm{LR}} = (\varepsilon_{p,\mathrm{LR}}, \varepsilon_{u,\mathrm{LR}})$. So vector addition property can apply on the solution diagram if the dividing lines of the wave patterns are chosen as co-ordinates. Consequently, new state variables are redefined as

$$\xi_e = \varepsilon_p + \varepsilon_u; \quad \xi_c = 2\sinh\left(\frac{\varepsilon_p}{2}\right) + \varepsilon_u$$

$$\eta_e = \varepsilon_p - \varepsilon_u; \quad \eta_c = 2\sinh\left(\frac{\varepsilon_p}{2}\right) - \varepsilon_u$$

and illustrated as

$$\xi_e = 0, \text{ left-going expansion fan;}$$

$$\xi_c = 0, \text{ left-going shock wave;}$$

$$\eta_e = 0, \text{ right-going expansion fan;}$$

$$\eta_c = 0, \text{ right-going shock wave}$$

and

$$\xi_e = 0 \text{ and } \xi_c = 0 \text{ represent the vector } \vec{\varepsilon}_{\mathrm{L}*}$$

$$\eta_e = 0 \text{ and } \eta_c = 0 \text{ represent the vector } \vec{\varepsilon}_{*\mathrm{R}}$$

Due to the property of vector addition, Equation (14), any state on the solution diagram, $\vec{\varepsilon}_{\mathrm{LR}}$, can be represented by two states on the lines $\xi = 0$ and $\eta = 0$. For example, the states of point P in the region of Type I can be divided into two components of point Q and R on the $\xi_e = 0$

Copyright © 2002 John Wiley & Sons, Ltd.

and $\eta_e = 0$, respectively, as shown in Figure 1,

$$\vec{\varepsilon}_{\mathrm{P}} = \vec{\varepsilon}_{\mathrm{R}} + \vec{\varepsilon}_{\mathrm{Q}}$$

if the area surrounded by points ORPQ is parallelism. Similarly, point P' can be represented by R and Q:

$$\vec{\varepsilon}_{\mathrm{P}'} = \vec{\varepsilon}_{\mathrm{R}} + \vec{\varepsilon}_{\mathrm{Q}'}$$

Since P and P′ lie on the line, $\xi_e = \varepsilon_p + \varepsilon_u = \text{constant}$, they will yield the same intermediate states if their right states are the same. As a result, the intermediate states can be determined by the following relations:

$$2\sinh(\tfrac{1}{2}\,\varepsilon_{p,*\mathrm{R}}) - \varepsilon_{u,*\mathrm{R}} = 0$$

$$\varepsilon_{p,*\mathrm{R}} + \varepsilon_{u,*\mathrm{R}} = \varepsilon_{p,\mathrm{LR}} + \varepsilon_{u,\mathrm{LR}} = \xi_{e,\mathrm{LR}}$$

or

$$2\sinh(\tfrac{1}{2}\,\varepsilon_{p,*\mathrm{R}}) + \varepsilon_{p,*\mathrm{R}} = \xi_{e,\mathrm{LR}}$$

In this way, a state net for any $\vec{\varepsilon}_{\mathrm{LR}}$ can be constructed on the solution diagram and the solutions of the Rieman problem can be easily obtained. Based on the present analysis and previous results, the resulting intermediate states are determined by, according to the wave patterns,

(1) Type I

$$2\sinh(\tfrac{1}{2}\,\varepsilon_{p,*\mathrm{R}}) + \varepsilon_{p,*\mathrm{R}} = \xi_{e,\mathrm{LR}} = \varepsilon_{p,\mathrm{LR}} + \varepsilon_{u,\mathrm{LR}}$$

(2) Type II

$$\varepsilon_p^* = 2\sinh^{-1}\left[\frac{\varepsilon_{u,\mathrm{LR}}}{4\cosh((1/4)\varepsilon_{p,\mathrm{LR}})}\right]$$

(3) Type III

$$2\sinh(\tfrac{1}{2}\,\varepsilon_{p,\mathrm{L}*}) + \varepsilon_{p,\mathrm{L}*} = \eta_{e,\mathrm{LR}} = \varepsilon_{p,\mathrm{LR}} + \varepsilon_{u,\mathrm{LR}}$$

(4) Type IV

$$\varepsilon_p^* = \tfrac{1}{2}\,\varepsilon_{u,\mathrm{LR}}$$

For the fast Godunov method, iteration is still necessary to solve the intermediate states for the cases of Types I and III. The general form of the equation is written as

$$f(x) = x + 2\sinh\left(\frac{x}{2}\right) - y$$

where y is given and x unknown. The initial guess is determined by the following third-order approximation,

$$f_3(x) = 2x_0 + \tfrac{1}{24}\,x_0^3 - y = 0$$

Copyright © 2002 John Wiley & Sons, Ltd.

and the second-order Newton–Raphson method is implemented,

$$f(x) = f(x_0) + f'(x_0)(x - x_0) + \tfrac{1}{2} f''(x_0)(x - x_0)^2 = 0$$

with

$$f'(x) = 1 + \cosh\left(\frac{x}{2}\right)$$

$$f''(x) = \frac{1}{2}\sinh\left(\frac{x}{2}\right)$$

The iteration number of the present so called fast Riemann solver for the convergence criteria being $f(x) < 10^{-7}$ is tested and summarized:

(1) $y < 0.3$, no iteration required,
(2) $y < 5$, one iteration required,
(3) $y < 20$, two iterations required.

It is worth noting that the range for $y < 20$ almost covers all the ranges of practical problem, since $y \equiv \xi_{e,\mathrm{LR}} \equiv \varepsilon_{p,\mathrm{LR}} + \varepsilon_{u,\mathrm{LR}}$ or $y \equiv \eta_{e,\mathrm{LR}} \equiv \varepsilon_{p,\mathrm{LR}} - \varepsilon_{u,\mathrm{LR}}$.

Due to the non-linearity of the Riemann problem it is difficult to describe the interactions among flow variables very clearly. However, the purposes can be achieved by linearizing the Riemann problem under the circumstances, $\varepsilon_u \approx \varepsilon_p \ll 1$.

It is interesting to discover that the approximate solutions of all wave patterns with second-order accuracy are the same and the approximate intermediate states of the Riemann

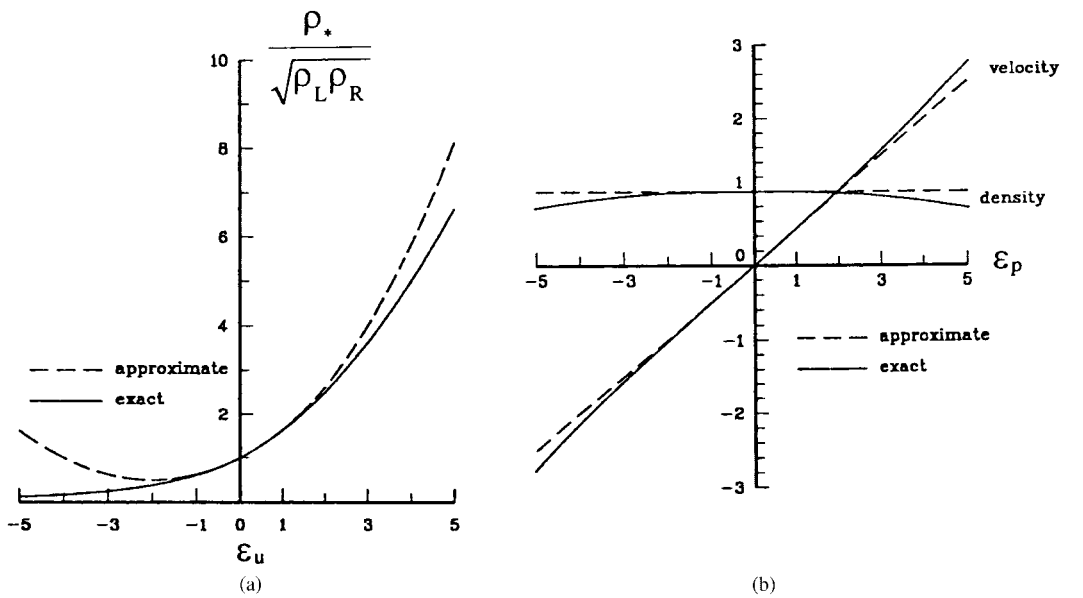

Figure 2. Approximate solution by small perturbation: (a) along ε_u; (b) along ε_p.

Copyright © 2002 John Wiley & Sons, Ltd.

problem are:

$$\rho_* = \sqrt{\rho_L \rho_R}(1 + \tfrac{1}{2}\varepsilon_u + \tfrac{1}{8}\varepsilon_u^2) \tag{15a}$$

$$u_* = \tfrac{1}{2}(u_L + u_R) + \tfrac{1}{2}c\varepsilon_p \tag{15b}$$

The density (or pressure) is only dependent on the perturbation of velocity (ε_u) while the velocity on the perturbation of density (ε_p), if the reference states are known. If $\sqrt{\rho_L \rho_R}$ is defined as the reference density of intermediate state, the term $(1 + \frac{1}{2}\varepsilon_u + \frac{1}{8}\varepsilon_u^2)$ can be considered as the compressibility effect resulting from the change of velocity; if $\frac{1}{2}(u_L + u_R)$ is defined as the reference velocity, the term $(\frac{1}{2}c\varepsilon_p)$ can be considered as the increment resulting from the change of density (or pressure). The comparisons between the intermediate states by small perturbation and exact solution are shown in Figure 2, and the error is not significant if ε_p and ε_u are less than 0.5.

5. NUMERICAL METHODS

It is well known that the Godunov method can be generalized to an algorithm that takes three independent steps (reconstruct, solve, average) in each time step. To achieve higher-order accuracy a better reconstruction such as linear function instead of piecewise constant is applied in the first step of the Godunov method. However, higher-order linear difference schemes will inevitably induce numerical oscillations. To avoid numerical oscillations several non-linear difference schemes with flux limiter such as the minmod, superbee and Van Leer schemes are tested and Van Leer Scheme shows the best performance in the single-equation case [7]. The general functional form of difference schemes can be represented as

$$\psi_{i+1/2}^L = \psi(r_{i+1/2}^L); \quad \psi_{i+1/2}^R = \psi(r_{i+1/2}^R)$$

in which $r_{i+1/2}^L$ and $r_{i+1/2}^R$ are defined as

$$r_{i+1/2}^L = \frac{u_{i+1} - u_i}{u_i - u_{i-1}}; \quad r_{i+1/2}^R = \frac{u_i - u_{i+1}}{u_{i+1} - u_{i+2}}$$

So, the first-order upwind scheme (1UD) is $\psi(r) = 0$ and the general linear second-order difference scheme is

$$\psi(r) = \frac{1+\kappa}{2} r + \frac{1-\kappa}{2}$$

where κ is constant, $\kappa = -1$ represents the central difference scheme (CD), for instance. And the functional form of the Van Leer scheme with limiter is represented as

$$\psi_{Van}(r) = \max\{0, \min[\tfrac{1}{2}(1+r), 2, 2r]\}$$

The detail derivations of the present numerical method will be omitted since the Godunov-type high-resolution schemes can be easily found in the book [4]. The difference scheme for

Copyright © 2002 John Wiley & Sons, Ltd.

system equations, Equation (2), can be written as

$$\tilde{U}_{i+1/2,\mathrm{L}} = U_i^n + \frac{1}{2}\left(I - \frac{\Delta t}{\Delta x} A_i\right) \Psi_{i+1/2}^{\mathrm{L}}(U_i^n - U_{i-1}^n), \tag{16a}$$

$$\tilde{U}_{i+1/2,\mathrm{R}} = U_{i+1}^n + \frac{1}{2}\left(I + \frac{\Delta t}{\Delta x} A_{i+1}\right) \Psi_{i+1/2}^{\mathrm{R}}(U_{i+1}^n - U_{i+2}^n) \tag{16b}$$

$$U_i^{n+1} = U_i^n - \frac{\Delta t}{\Delta x}[F^N(\tilde{U}_{i+1/2,\mathrm{L}}, \tilde{U}_{i+1/2,\mathrm{R}}) - F^N(\tilde{U}_{i-1/2,\mathrm{L}}, \tilde{U}_{i-1/2,\mathrm{R}})] \tag{16c}$$

where I is unit matrix and $\Psi_{i+1/2}^{\mathrm{L}}$ and $\Psi_{i+1/2}^{\mathrm{R}}$ are limiter matrix of flux vector, which have the same functional form as that of single equation,

$$\Psi(r_\rho, r_{\rho u}) = \begin{pmatrix} \psi(r_\rho) & 0 \\ 0 & \psi(r_{\rho u}) \end{pmatrix} \tag{16d}$$

For a Riemann solver to be called fast it has to be comparable to the popularly used approximate Riemann solver which get rid of iterations for the solution of the Riemann problem. Among them, Roe scheme is one of the most popular schemes in the gas dynamics. As a result, Roe scheme is utilized and formulated for the present water-hammer problem with the numerical flux being [7]

$$F_{i+1/2}^{\mathrm{R}} = \tfrac{1}{2}(F(U_{\mathrm{L}}) + F(U_{\mathrm{R}})) - \tfrac{1}{2}\hat{R}|\hat{\Lambda}|\hat{R}^{-1}(U_{\mathrm{R}} - U_{\mathrm{L}})$$

where the superscript R stands for the Roe scheme, $\hat{R}$ and $\hat{\Lambda}$ are the eigenvector and eigenvalue matrix of the approximately constructed Jacobian matrix $\hat{A}$, respectively. The construction of approximate Jacobian matrix $\hat{A}$ from A has to satisfy the Rankin–Hugoniot relation, consistency and hyperbolicity and can be referenced in Reference [4].

6. ERROR ANALYSIS

The error analysis can be performed by using the Von Neumann method to validate that the numerical method is second-order accuracy in space and time. For convenience, $G = \rho u$ is defined in the derivations. Considering the general linear second-order difference scheme, the propagation of small perturbation of the numerical method would be

$$\begin{pmatrix} \delta\rho_i^{n+1} \\ \delta G_i^{n+1} \end{pmatrix} = \begin{pmatrix} a_{\rho\rho} & a_{\rho G} \\ a_{G\rho} & a_{GG} \end{pmatrix} \begin{pmatrix} \delta\rho_i^n \\ \delta G_i^n \end{pmatrix} \tag{17}$$

where

$$a_{\rho\rho} = 1 - \frac{c\Delta t}{2\Delta x}(1 - M^2)(-D + 2 - D^{-1} + D_s) + \frac{c^2\Delta t^2}{2\Delta x^2}(1 - M^2)(MD_a + D_s)$$

Copyright © 2002 John Wiley & Sons, Ltd.

$$a_{\rho G} = -\frac{\Delta t}{2\Delta x}\left[M(-D+2-D^{-1}+D_s)+(D-D^{-1}+D_a)\right] + \frac{c\Delta t^2}{2\Delta x^2}\left[(1+M^2)D_a+2MD_s\right)$$

$$a_{G\rho} = c^2(1-M^2)a_{\rho G}$$

$$a_{GG} = 1-\frac{c\Delta t}{2\Delta x}\left[(1+M^2)(-D+2-D^{-1}+D_s)+2M(D-D^{-1}+D_a)\right] + \frac{c^2\Delta t^2}{2\Delta x^2}\left[(1+3M^2)D_a+M(3+M^2)D_s)\right]$$

in which $M = u_0/c$ and the difference operators D, D_a and D_s are

$$D\delta\rho_i = \delta\rho_{i+1}$$

$$D_a = \frac{1-\kappa}{4}(-D^2+2D-2D^{-1}+D^{-2})$$

$$D_s = \tfrac{1}{4}[2(1+\kappa)(D-2+D^{-1})+(1-\kappa)(D^2-2D+2-2D^{-1}+D^{-2})]$$

By transforming the difference operations into differential relations based on the principle of Tailor expansion, the derived modified equations are

$$\frac{\partial\delta\rho}{\partial t}+\frac{1}{2}\frac{\partial^2\delta\rho}{\partial t^2}\Delta t+\frac{1}{6}\frac{\partial^3\delta\rho}{\partial t^3}\Delta t^2-\frac{c^2\Delta t}{2}(1-M^2)\left[\frac{\partial^2\delta\rho}{\partial x^2}-\frac{M(1-\kappa)}{2}\frac{\partial^3\delta\rho}{\partial x^3}\Delta x\right] + \frac{\partial\delta G}{\partial x}+\frac{-1+3\kappa}{12}\frac{\partial^3\delta G}{\partial x^3}\Delta x^2-\frac{c\Delta t}{2}\left[2M\frac{\partial^2\delta G}{\partial x^2}-\frac{1+M^2}{2}(1-\kappa)\frac{\partial^3\delta G}{\partial x^3}\Delta x\right]=0$$

and

$$\frac{\partial\delta G}{\partial t}+\frac{1}{2}\frac{\partial^2\delta G}{\partial t^2}\Delta t+\frac{1}{6}\frac{\partial^3\delta G}{\partial t^3}\Delta t^2+c^2(1-M^2)\left[\frac{\partial\delta\rho}{\partial x}+\frac{(-1+3\kappa)}{12}\frac{\partial^3\delta\rho}{\partial x^3}\Delta x^2\right] - \frac{c^3\Delta t(1-M^2)}{2}\left[2M\frac{\partial^2\delta\rho}{\partial x^2}-\frac{1+M^2}{2}(1-\kappa)\frac{\partial^3\delta\rho}{\partial x^3}\Delta x\right] + c\left[2M\frac{\partial\delta G}{\partial x}-\frac{M(-1+3\kappa)}{6}\frac{\partial^3\delta G}{\partial x^3}\Delta x^2\right] - \frac{c^2\Delta t}{2}\left[(1+3M^2)\frac{\partial^2\delta G}{\partial x^2}-\frac{M(3+M^2)}{2}(1-\kappa)\frac{\partial^3\delta G}{\partial x^3}\Delta x\right]=0$$

Copyright © 2002 John Wiley & Sons, Ltd.

With the relations

$$\frac{\partial^2 \delta U}{\partial t^2} = A^2 \frac{\partial^2 \delta U}{\partial x^2}$$

the truncation error of the numerical method are easily obtained

$$\begin{aligned}
\mathrm{TE}_\rho &= \frac{1}{6}\frac{\partial^3 \delta\rho}{\partial t^3}\Delta t^2 + \frac{c\mathrm{Cr}M(1-M^2)}{4}(1-\kappa)\frac{\partial^3 \delta\rho}{\partial x^3}\Delta x^2 \\
&\quad + \left[\frac{-1+3\kappa}{12} + \frac{\mathrm{Cr}(1+M^2)}{4}(1-\kappa)\right]\frac{\partial^3 \delta G}{\partial x^3}\Delta x^2 + \mathrm{HOT} \\
\mathrm{TE}_G &= \frac{1}{6}\frac{\partial^3 \delta G}{\partial t^3}\Delta t^2 + c^2(1-M^2)\left[\frac{-1+3\kappa}{12} + \frac{\mathrm{Cr}(1+M^2)}{4}(1-\kappa)\right]\frac{\partial^3 \delta\rho}{\partial x^3}\Delta x^2 \\
&\quad + cM\left[\frac{-1+3\kappa}{6} + \frac{\mathrm{Cr}(1+3M^2)}{4}(1-\kappa)\right]\frac{\partial^3 \delta G}{\partial x^3}\Delta x^2 + \mathrm{HOT}
\end{aligned}$$

in which HOT denotes higher-order term. For the 1UD, the truncation error of the numerical method would be, as expected, first-order in accuracy

$$\begin{aligned}
\mathrm{TE}_\rho &= \frac{c}{2}(1-M^2)(c\Delta t - \Delta x)\frac{\partial^2 \delta\rho}{\partial x^2} + M\left(c\Delta t - \frac{\Delta x}{2}\right)\frac{\partial^2 \delta G}{\partial x^2} + \mathrm{HOT} \\
\mathrm{TE}_G &= \frac{c^2 M(1-M^2)}{2}(c\Delta t - \Delta x)\frac{\partial^2 \delta\rho}{\partial x^2} + \frac{c(1+M^2)}{2}cM\left(\frac{1+3M^2}{1+M^2}c\Delta t - \Delta x\right)\frac{\partial^2 \delta G}{\partial x^2} + \mathrm{HOT}
\end{aligned}$$

7. TEST PROBLEMS AND COMPUTATIONAL RESULTS

To test the developed numerical method, two sample problems are investigated. One is the typical Riemann problem: a valve, by which two discontinuous states are separated in a pipe, is opened abruptly and the other is the water-hammer problem: the propagation of pressure wave is simulated in a pipe with the valve at downstream being opened and closed periodically. Moreover, some sensitivity studies such as the effects of pressure strength and time step are also performed to examine the difference schemes.

For demonstrations, the second type of the Riemann problem is taken into account. The computational cells are set to $N = 200$, and sound speed $c = 1$. The initial conditions of Riemann problem are set to be

$$\begin{aligned}
p = 1, \quad u = 0, \quad &\text{if } x < 0 \\
p = 1, \quad u = -1 \quad &\text{if } x > 0
\end{aligned}$$

Two out-going shocks will be formed in this circumstance. Figure 3 shows the computational results at $t = 0.25$ with $\mathrm{Cr} = 0.5$ for the 1UD, CD and Van Leer schemes, respectively. The

Copyright © 2002 John Wiley & Sons, Ltd.

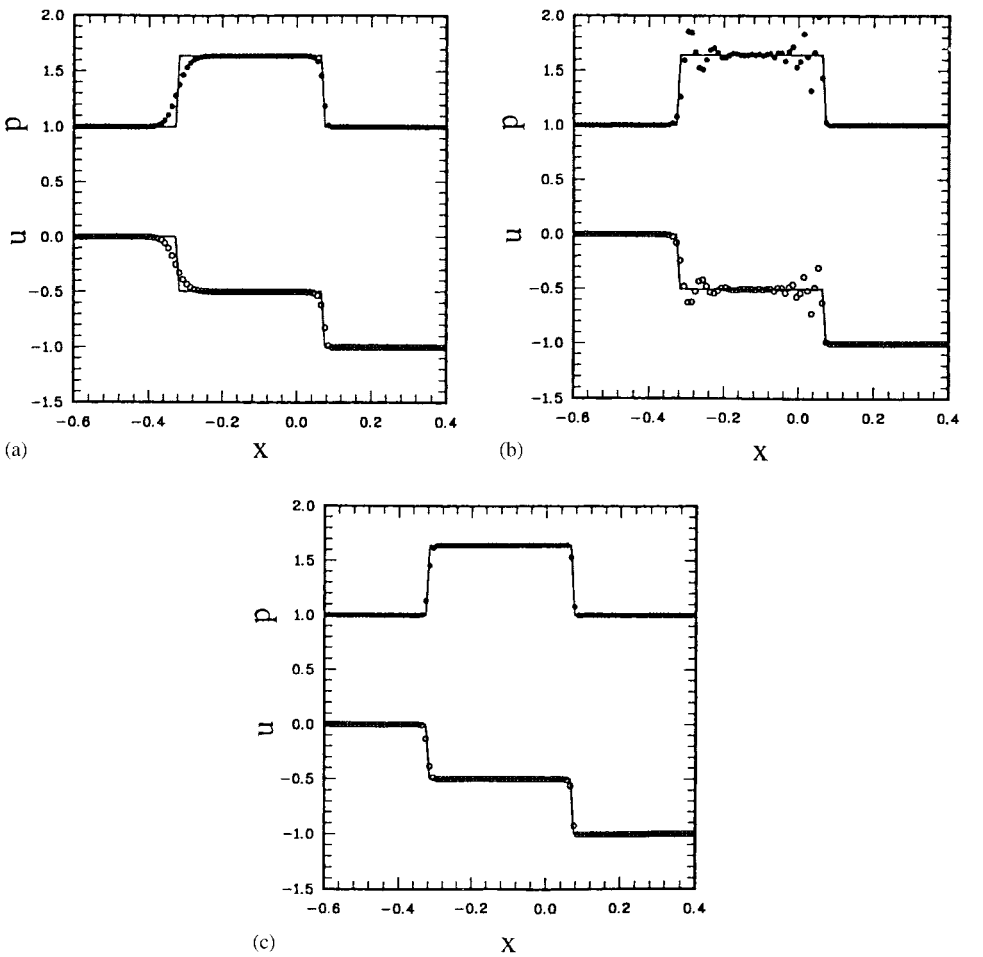

Figure 3. Distribution of pressure and velocity with $\mathrm{Cr} = 0.5$ for the Riemann problem of wave pattern type II by: (a) 1UD; (b) CD; and (c) Van Leer.

Courant number, Cr, is defined as

$$\mathrm{Cr} = \frac{|\lambda|_{\max}\Delta t}{\Delta x}$$

It is noted that the agreements are well for the right-going shock but significant dissipation can be found for the left-going shock by using the 1UD scheme (Figure 3(a)). There are serious oscillations before and after the shock for the CD but the simulation results by the Van Leer scheme are quite well. All the schemes, linear or non-linear, are able to obtain the same wave speed and the intermediate state of the Riemann problem, which means the Rankine–Hugoniot relation is satisfied. Generally, the results show similar characteristics of the difference schemes as observed in the gas dynamics.

The other test problem is to simulate the water-hammer in a pipe by closing and opening of valve at downstream. The pressure waves caused by the action of the valve then start

Copyright © 2002 John Wiley & Sons, Ltd.

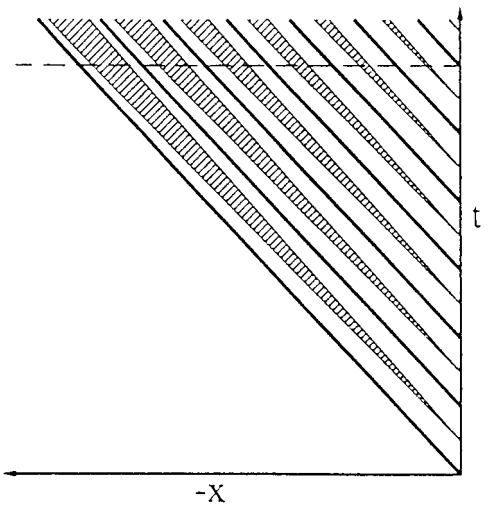

Figure 4. Schematic diagram of wave-form propagating on the x–t plane.

to propagate toward upstream along the pipe. The time-dependent pressure boundary condition is assumed to be a square wave at downstream valve position, $x = 10$. Figure 4 shows the schematic diagram of the waveform propagating on the x–t plane. The thick solid lines represent the shock wave caused by valve closing, while the shadow regions the expansion fans caused by valve opening. Since the speed of shock and expansion fans are different, shock and expansion fan will get closer and expansion fan will expand wider as the waves propagate along the pipe. The horizontal dotted line in the figure explains the distribution of the waves for a specified time. In the calculation, sound speed is set to $c = 1$, computational cells $N = 200$ and period of pressure variation $30\Delta x/c$.

Figure 5 illustrates the results with $\Delta p = 0.01$ and $\mathrm{Cr} = 1.0$ for the schemes of 1UD, CD and Van Leer, respectively. The solid line shown in the figures is a reference result by the MOC. It is noted that the speed of expansion fan and shock are the same and the MOC makes no differences between expansion fan and shock. The exact solutions (dash line) for this problem are also calculated to benchmark the results. The results show that the Godunov method, incorporated with Van Leer scheme, can tell the differences between expansion fan and shock effectively even when the strength of pressure is only 0.01. The strength of shock sustains but the gradient of expansion fan is gradually reduced as the wave propagate, which is the same case as shown in Figure 4. The strength predicted by the 1UD is dissipated a little because there is more numerical dissipation inherent in the scheme as shown in Figure 5(a). CD is expected to have oscillation after sharp gradient because of phase lagging as shown in Figure 5(b). Van Leer scheme predicts shock and expansion fan accurately as shown in Figure 5(c). These results are consistent with the previous discussions for the Riemann problem in gas dynamics. Figure 6 shows similar results for the cases with $\mathrm{Cr} = 0.5$.

Moreover, the effects of the strength of pressure variation are considered. Similar computational results with $\Delta p = 0.1$ and $\mathrm{Cr} = 1.0$ for the 1UD, CD and Van Leer scheme are shown in Figure 7. Again, because of numerical dissipation in the 1UD scheme, expansion wave and

Copyright © 2002 John Wiley & Sons, Ltd.

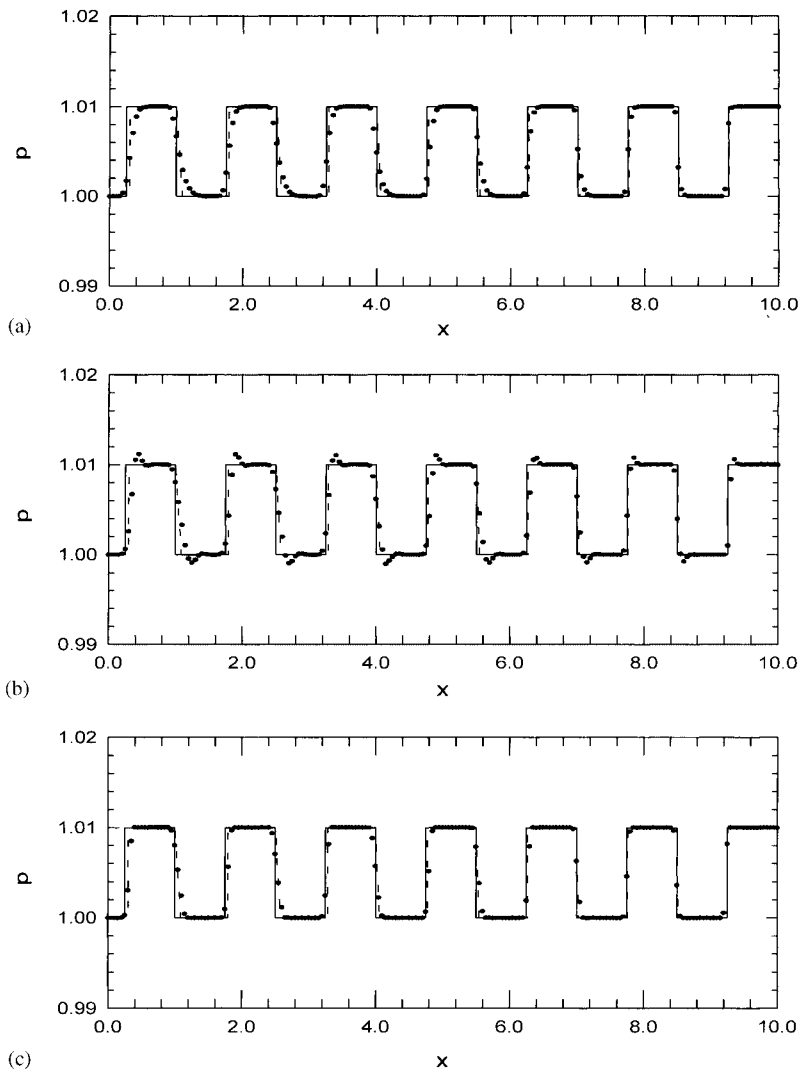

Figure 5. Simulation results of water-hammer with $\Delta p = 0.01$, $\mathrm{Cr} = 1.0$ by: (a) 1UD; (b) CD; and (c) Van Leer.

shock become coupled and the amplitude is significantly reduced as shown in Figure 7(a). Figure 7(b) shows the oscillations predicted by the CD and the oscillation amplitude is increased as the pressure variation increased. The simulation case with $\Delta p = 0.1$ and $\mathrm{Cr} = 0.5$ is also performed to demonstrate the effects of time step as shown in Figure 8. It shows that the Van Leer scheme agrees well with the exact solution, especially for the shock speed and the expansion behaviour of expansion wave. Other phenomena are the same as that for the case of $\Delta p = 0.1$ and it is summarized that 1UD and CD are not able to predict the wave propagation accurately under the present conditions. Therefore, to obtain reasonably accurate

Copyright © 2002 John Wiley & Sons, Ltd.

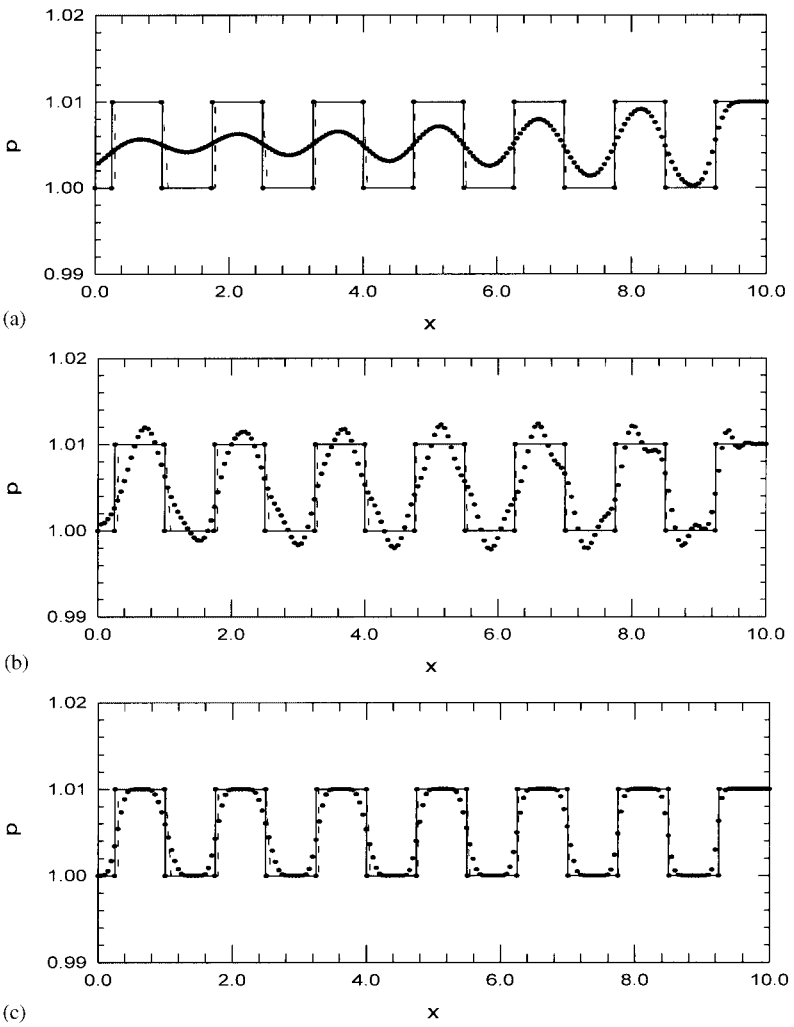

Figure 6. Simulation results of water-hammer with $\Delta p = 0.01$, $\mathrm{Cr} = 0.5$ by: (a) 1UD; (b) CD; and (c) Van Leer.

simulation results for the water-hammer problem, non-linear second-order difference schemes with flux limiter such as Van Leer scheme could be a candidate to be implemented.

To benchmark the computational efficiency of the present fast Riemann solver, the arithmetic operation numbers for each cell are counted for the programs coded by Roe's scheme and the present one. The statistical results are shown in Table I. It shows that the present Godunov method has a few more arithmetic operations like division, addition and exponential but far less operation of multiplication is needed. A typical fluid transient problem, which is initially steady and induced by quickly closing valve at downstream in a reservoir-pipe-valve system, is simulated for 100 s to test the required CPU time. The results show it takes 22.46 s for the present exact Riemann solver and 21.92 s for the Roe's approximate Riemann

Copyright © 2002 John Wiley & Sons, Ltd.

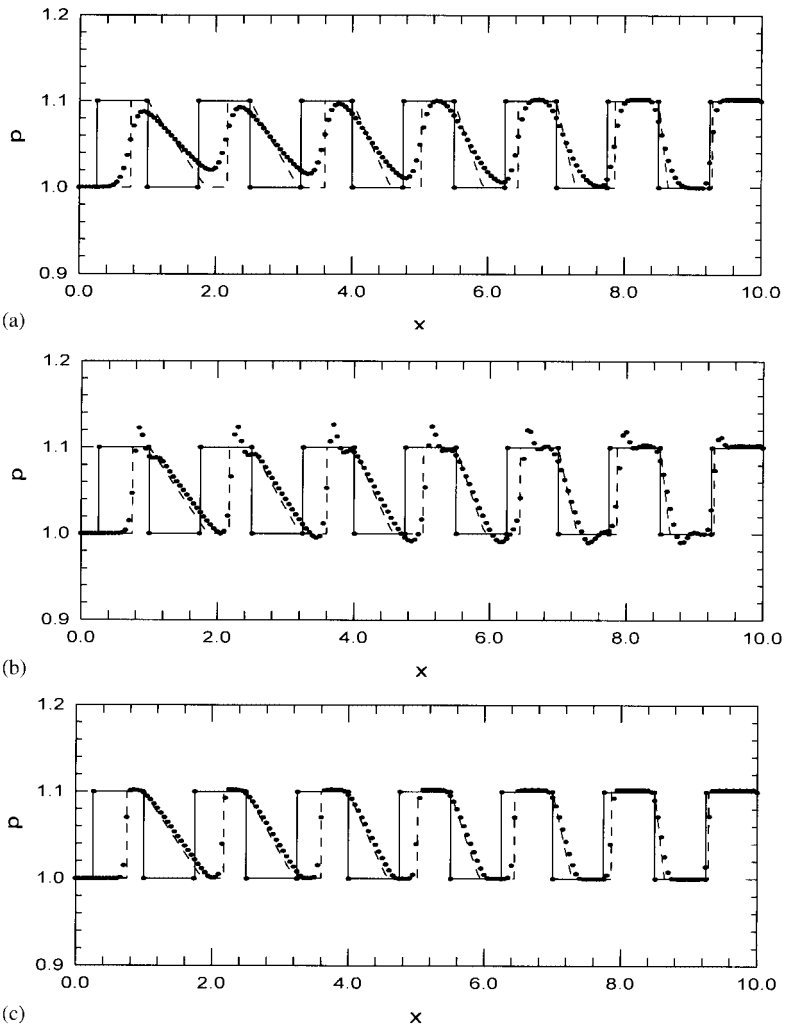

Figure 7. Simulation results of water-hammer with $\Delta p = 0.1$, $\mathrm{Cr} = 1.0$ by: (a) 1UD; (b) CD; and (c) Van Leer.

solver. Generally speaking, the present Godunov method requires a little more arithmetic operation and CPU time but is able to get more accurate computational results than Roe's scheme.

8. CONCLUSIONS

An efficient Godunov-type numerical method with second-order accuracy to simulate water-hammer problem for piping are developed in this paper. An intriguing solution diagram of the Riemann problem for the water-hammer equations is proposed with the properly selected

Copyright © 2002 John Wiley & Sons, Ltd.

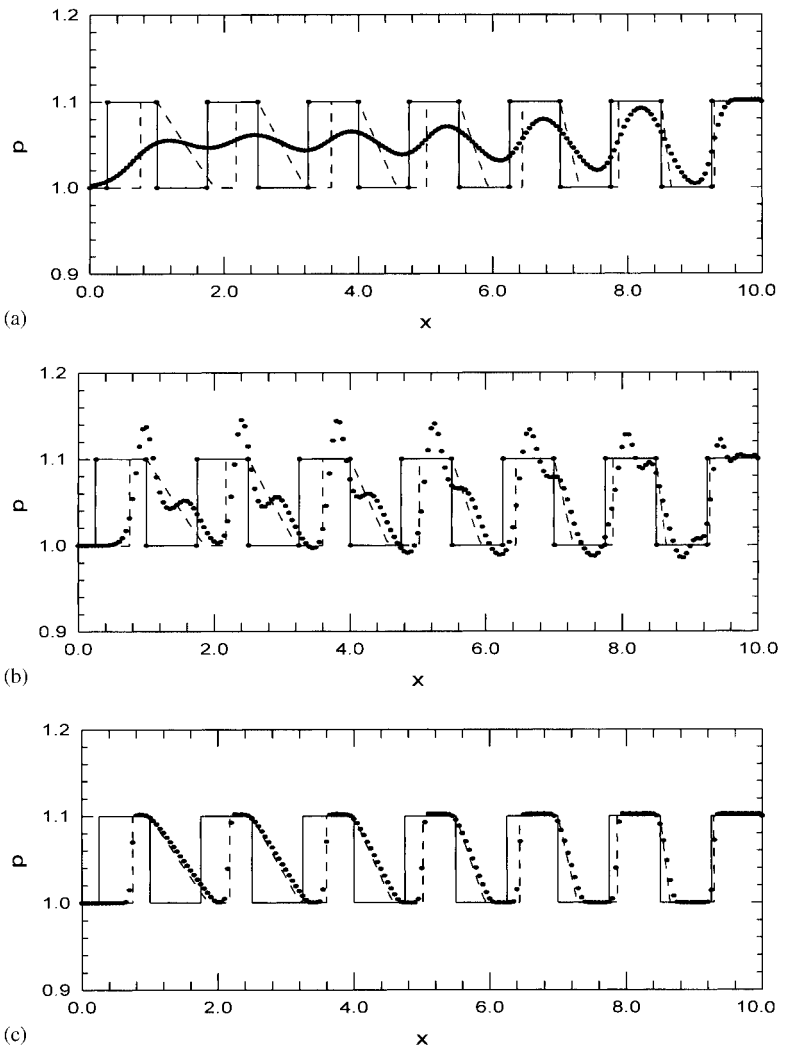

Figure 8. Simulation results of water-hammer with $\Delta p = 0.1$, $\mathrm{Cr} = 0.5$ by: (a) 1UD; (b) CD; and (c) Van Leer.

Table I. Comparisons of arithmetic operation numbers between Roe scheme and the present numerical method.

	+	−	*	/	$\sqrt{}$	Log	Exp
Roe	14	12	32	4	2	0	0
Present	12	15	18	9	2	2	6

Copyright © 2002 John Wiley & Sons, Ltd.

dimensionless parameters $(\varepsilon_u, \varepsilon_p)$ being co-ordinates. On the solution diagram, any states can be constituted by vector addition based on the lines $\xi = 0$ and $\eta = 0$ being axis (Equation (14)). Furthermore, based on the solution diagram and the property of vector addition, the fast Riemann solver can be constructed for reasonably practical ranges with limited iterations and expected to be comparable to the Roe's method in efficiency. Moreover, it is shown that the intermediate state of density (or pressure) is only dependent on the perturbation of velocity, while the velocity on the perturbation of density by small perturbation analysis (Equation (15)). Some linear and non-linear second-order difference schemes are incorporated into the numerical method as had been done in gas dynamics to test the suitability. Van Leer scheme is shown to be the best one in the present study, which is similar to previous experiences.

The approaches developed in the present study can be extended to solve the Riemann problem for gas dynamics in which there are three governing equations instead of two, and the paper will appear in the near future.

ACKNOWLEDGEMENTS

The authors would like to thank Dr H. C. Yang, group leader of Chung-Shun Institute of Science and Technology and Mr C. M. Hsu, leader of Energy Lab., Power Research Institute, Taiwan Power Company, for their support to the research.

REFERENCES

1. Benjamin Wylie E, Streeter VL. *Fluid Transients in Systems*. Prentice-Hall, Inc.: Englewood Cliffs, NJ, 1993.
2. Bisgarrd C, Sorensen HH, Spangenberg S. A finite element method for transient compressible flow in pipelines. *International Journal for Numerical Methods in Fluid Flow* 1987; **7**:291–303.
3. Ng KC, Yap C. An investigation of pressure transients in pipelines with two-phase bubbly flow. *International Journal for Numerical Methods in Fluid Flow* 1989; **9**:1207–1219.
4. Hirsh C. Numerical computation of internal and external flows. *Computational Methods for Inviscid and Viscous Flows*, vol. 2. Wiley: New York, 1990.
5. Sod GA. A survey of several finite difference methods for systems nonlinear hyperbolic conservation law. *Journal of Computational Physics* 1978; **27**:1–31.
6. Whitman GB. *Linear and Nonlinear Waves*. Wiley: New York, 1974.
7. Hwang YH, Chung NM. *Establishment of an Analyzing Methodology for Water Hammer Phenomena in the Piping of Power Plant-Numerical Analyses and Improvements with the RELAP5 Code*, *Project No*. 4321-07, Taiwan Power Company, 1998 (in Chinese).

Copyright © 2002 John Wiley & Sons, Ltd.